Journal of Power Sources 195 (2010) 912–918

Contents lists available at ScienceDirect

Journal of Power Sources

journal homepage: www.elsevier.com/locate/jpowsour

Microstructure and electrochemical double-layer capacitance of carbon electrodes prepared by zinc chloride activation of sugar cane bagasse

Thomas E. Rufford*, Denisa Hulicova-Jurcakova, Kiran Khosla, Zhonghua Zhu, Gao Qing Lu

ARC Centre of Excellence for Functional Nanomaterials, School of Chemical Engineering and Australian Institute for Bioengineering and Nanotechnology, The University of Queensland, 4072 Queensland, Australia

ARTICLE INFO

Article history:
Received 18 May 2009
Received in revised form 14 July 2009
Accepted 13 August 2009
Available online 25 August 2009

Keywords:
Double-layer capacitor
Activated carbon
Bagasse
Agricultural waste
Energy storage

ABSTRACT

Activated carbons for supercapacitor electrodes are prepared from sugar cane bagasse using chemical activation with $ZnCl_2$. The $ZnCl_2$ activation of bagasse is studied using thermogravimetric analysis and the carbon pore structures are characterised using N_2 and CO_2 adsorption. In two-electrode, sandwich-type supercapacitor cells containing 1 M H_2SO_4 the sugar cane bagasse carbons (SCCs) exhibit specific energy up to 10 Wh kg^{-1} and specific capacitance close to 300 F g^{-1}. The electrochemical performance of the SCCs is attributed to their high specific surface area and the development of mesopores with $ZnCl_2$ impregnation ratios of 1 or greater. By contrast, the pyrolysis of bagasse without $ZnCl_2$ produces a carbon with low specific capacitance. The SCC prepared with a $ZnCl_2$ ratio of 3.5 shows the most stable electrochemical performance at fast charge–discharge rates.

1. Introduction

Road transportation is dominated by vehicles operating on fossil-fuel based internal combustion engines. A growing global energy demand and an increased awareness of the environmental impacts of fossil-fuel combustion, including the emission of greenhouse gases and local air pollutants, have driven the search for alternative transportation fuels. A key challenge in the development of low-emission vehicles is the development of energy-storage devices with high specific power and specific energy. Supercapacitors, or electrochemical double-layer capacitors, are a promising high power technology with the ability to be meet peak power demands in fuel cell electric vehicles.

Supercapacitors predominantly store energy by the accumulation of charge at electrodes by electrostatic forces [1], without reliance on charge-transfer reactions like in the operation of conventional batteries. The electrochemical double-layer phenomena in supercapacitors have the potential to achieve stable and reversible charge cycling for a long device life, and high power rates. The specific energy of a supercapacitor is, however, a fraction of a conventional battery. The specific energy of a supercapacitor is proportional to the specific capacitance of the cell, which is influenced strongly by the surface area of the electrodes. Activated carbons with high surface areas, typically from petroleum coke or coal, are the most common electrode materials used in supercapacitors. The carbon electrodes are a significant material cost in a supercapacitor device [2] and the development of low-cost carbons with high specific energy and specific power is key to the widespread application of supercapacitors.

A recent trend in carbon supercapacitor electrodes has seen the use of biomass waste materials to produce activated carbons. Supercapacitors with carbon electrodes derived from biomass materials such as seaweed biopolymers [3], waste coffee beans [4,5], firwood [6], corn grains [7], banana fibres [8], and sugar cane bagasse [9] have been reported, as summarised in Table 1. The choice of carbon precursor and activation conditions determine the electrochemical performance, with carbon surface area, pore-size distribution, electrical conductivity and the presence of electrochemically active surface functional groups all affecting double-layer capacitance.

Sugar cane bagasse is a by-product from the milling of sugar cane and large quantities of this waste material are produced each milling season in Australia and other countries that produce sugar cane. Activated carbons prepared from sugar cane bagasse have been studied for applications such as waste water treatment [10,11] and gold extraction [12]. In 2008, Konno et al. [9] reported the electrochemical double-layer capacitance of a series of activated carbons prepared by NaOH activation of sugar cane wastes. Double-layer capacitance was reported to increase with both the specific surface area and the average pore width of the NaOH activated sugar cane carbons, with higher ratios of NaOH to sugar cane

* Corresponding author. Tel.: +61 7 33466201; fax: +61 7 33654199.
E-mail addresses: tomrufford@yahoo.com.au, t.rufford@uq.edu.au (T.E. Rufford).

0378-7753/$ – see front matter © 2009 Elsevier B.V. All rights reserved.
doi:10.1016/j.jpowsour.2009.08.048

Table 1
Survey of activated carbons from biomass precursors for electrode materials in supercapacitors. Capacitance reported here is the three-electrode equivalent for a single electrode.

Carbon source	Activation method	S_{BET} ($m^2\,g^{-1}$)	Capacitance ($F\,g^{-1}$)	Electrolyte	Ref.
Sugar cane bagasse[a]	NaOH	2871	109	1 M H_2SO_4	[9]
Banana fibres	$ZnCl_2$	1097	296[b]	1 M Na_2SO_4	[8]
Banana fibres	KOH	686	264[b]	1 M Na_2SO_4	[8]
Fir wood	KOH	1064	180	0.5 M H_2SO_4	[6]
Fir wood	Steam	1016	110	0.5 M H_2SO_4	[6]
Seaweed biopolymer	Thermal	273	198	1 M H_2SO_4	[3]
Corn grain	KOH	3199	257	6 M KOH	[7]
Coffee grounds	$ZnCl_2$	1019	368	1 M H_2SO_4	[4]

[a] For activated carbon from sugar cane pith prepared with a NaOH to bagasse ratio of 6 [9].
[b] The two-electrode specific capacitance values published in reference [8] have been converted to the three-electrode equivalent for a single electrode.

producing carbons with average pore widths greater than 1 nm [9].

Chemical activation using $ZnCl_2$, instead of NaOH, is well known to produce activated carbons with pores wider than 1 nm [13,14]. This study reports the characterisation and electrochemical performance of activated carbons prepared by the $ZnCl_2$ activation of sugar cane bagasse. The effects of the ratio of $ZnCl_2$ to bagasse, as well as activation temperature, on pore development and subsequently electrochemical performance are discussed.

2. Experimental methods

2.1. Activated carbon preparation

Sugar cane bagasse was rinsed in hot water at 100 °C for 8 h, filtered, and then air-dried at 100 °C for 48 h. In a typical synthesis experiment 2 g of bagasse was mixed with $ZnCl_2$ in 20 mL of distilled water. Activated carbons were prepared using $ZnCl_2$ to bagasse weight ratios of 0, 1, 2, and 3.5. The mixture was stirred at room temperature for 4 h and then dried in an oven at 100 °C. Carbonisation was performed in a tube furnace under a N_2 gas flow and at a heating rate of 5 °C min^{-1} to 900 °C. The maximum temperature was held for 1 h. The carbonized samples were washed in 0.2 M HCl, rinsed in distilled water, filtered and then dried to obtain the activated sugar cane carbons (SCCs). These samples are referred to as SCC-0, SCC-1, SCC-2, and SCC-3.5 with reference to the $ZnCl_2$ to bagasse weight ratio. Activated carbon SCC-1-750 was prepared by the same method described above with a $ZnCl_2$ to bagasse ratio of 1 and a maximum activation temperature of 750 °C.

2.2. Carbon characterisation

The carbons were characterised by N_2 adsorption at −196 °C using the Quadrasorb *SI* and CO_2 adsorption at 0 °C using the Autosorb 1-C (both instruments from Quantachrome). The specific surface areas (S_{BET}) were calculated from N_2 adsorption isotherms using the Brunauer–Emmett–Teller (BET) equation. The micropore and mesopore/external surface areas were obtained by the *t*-plot method, with carbon black (Mitsubishi Black #32) used as the reference sample in the *t*-plot analysis. Narrow micropore volumes were calculated from the CO_2 adsorption isotherms using the Dubinin–Radushkevich (DR) equation. Pore-size distributions were calculated using non-local density functional theory (DFT) methods for N_2 and CO_2 adsorption in carbon slit pores (using algorithms supplied in the Quadrawin 2.0 software).

Thermal gravimetric analysis (TGA) was conducted with a Mettler Toledo TGA/DSC1 in N_2 or air (flowrate of 20 mL min^{-1}) at a heating rate of 5 °C min^{-1}. X-ray photoelectron spectroscopy (XPS) was performed on a ESCALAB220i-XL (VG Scientific, UK) instrument that had a monochromated Al Kα excitation source. Wide survey spectra were collected with a pass energy of 100 eV and high-resolution spectra were collected for C1s, O1s and N1s regions with a pass energy of 20 eV. Quantitative analysis was undertaken with CASAXPS software after Shirley background subtraction.

2.3. Electrochemical measurements

Electrodes were prepared by mixing 90 wt.% activated carbon, 5 wt.% carbon black (Mitsubishi #32) and 5 wt.% polyvinylidene-fluoride in N-methyl pyrrolidone to form slurry. The slurry was painted in a 1 cm^2 area on titanium strips, with typically 3 mg active material applied to each electrode. Sandwich-type electrochemical cells were constructed, with two symmetrical carbon electrodes separated by glassy fibre paper, and the electrodes were immersed in 1 M H_2SO_4 electrolyte.

Cyclic voltammetry (CV) and galvanostatic charge–discharge cycles (GC) were measured in the voltage range 0–1 V (Solartron 1480 Multistat). Cyclic voltammetry was performed at scan rates of 5–50 mV s^{-1} and GC cycles were measure at current loads of 0.05–50 A g^{-1}. Specific capacitances (C) were calculated per single electrode as the three-electrode cell equivalent [15]. As per the convention for the construction of Ragone plots the specific capacitances of two-electrode cells (C_{2E}) were used in the calculation of specific energies ($E = C_{2E}U^2/2$), where U is the voltage in which the *IR* drop is omitted. Specific power was calculated from the formula $P = 0.5\,IU\,m^{-1}$, where I is the current and m the total mass of two working electrodes.

3. Results and discussion

3.1. Thermal analysis

The TGA weight-loss curves in Fig. 1 for (a) bagasse and (b) bagasse + $ZnCl_2$ (weight ratio $ZnCl_2$ to bagasse of 1) in a N_2 atmosphere are distinctly different. To highlight the temperatures at which mass-loss steps occur, the differential curves (dTGA/dt) are included in Fig. 1. The bagasse presents one continuous region of weight loss from 200 to 400 °C, with a dTGA/dt peak at approximately 340 °C. These results are consistent with the thermal characteristics of bagasse reported by Nassar et al. [16] and Munir et al. [17]. The bagasse weight-loss processes occurring below 400 °C are associated with dehydration and release of volatiles from the cellulosic structure [16,18]. The weight losses at temperatures less than 100 °C for bagasse and bagasse + $ZnCl_2$ are due to water evaporation.

In contrast to the thermal response of untreated bagasse, the thermal analysis of the bagasse + $ZnCl_2$ presents two regions of weight loss. The complex thermal response of bagasse + $ZnCl_2$ shown in Fig. 1b is consistent with results reported for the $ZnCl_2$ activation of other biomass materials [18,19]. The first weight-loss step from 150 to 210 °C is associated with the dehydration of the carbon precursor, a process which is promoted by the Lewis acid nature of $ZnCl_2$, and the volatilization of cellulosic fractions

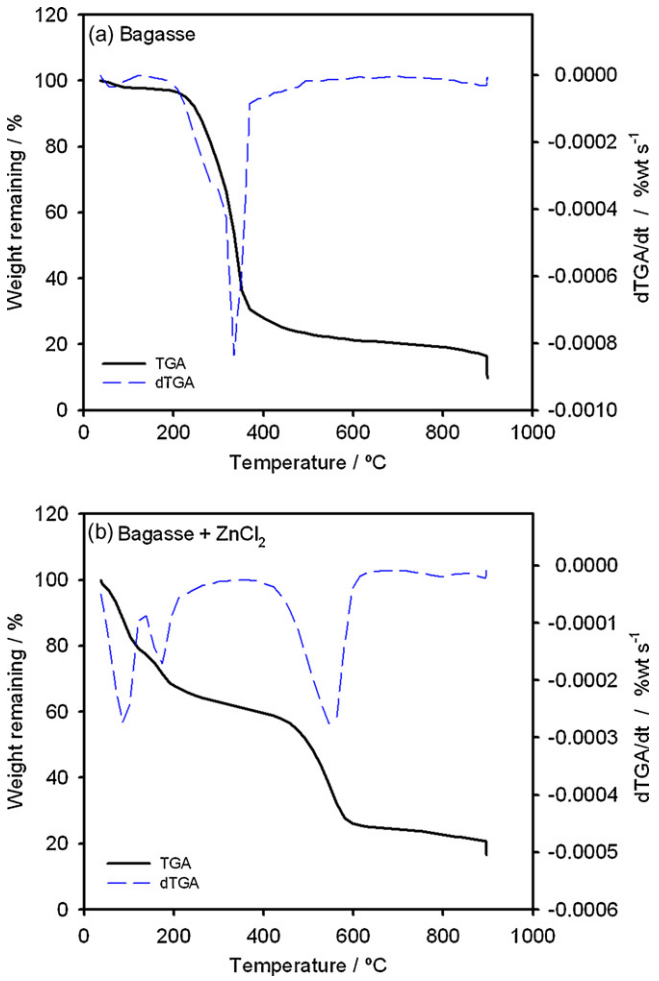

Fig. 1. Thermal gravimetric analyses (TGA) in N_2 of (a) sugar cane bagasse and (b) sugar cane bagasse + $ZnCl_2$.

of the bagasse [18]. The second weight-loss step at 420–620 °C includes the volatilization of $ZnCl_2$ [18] and carbon mass-loss via active pyrolysis and aromatic condensation reactions. Condensation reactions promoted by $ZnCl_2$ reduce tar formation and carbon gasification, which results in higher activated carbon yields than activation without $ZnCl_2$ [20,21]. The carbon yields from sugar cane bagasse are included in Table 2.

3.2. Textural properties and surface group analysis

To understand the influence of activation conditions on the development of pore structure in carbons prepared from sugar cane bagasse, the activated carbons were characterised by N_2 and CO_2 sorption analyses. The N_2 sorption isotherms for sugar cane bagasse carbons prepared in this work are presented in Fig. 2. The carbon

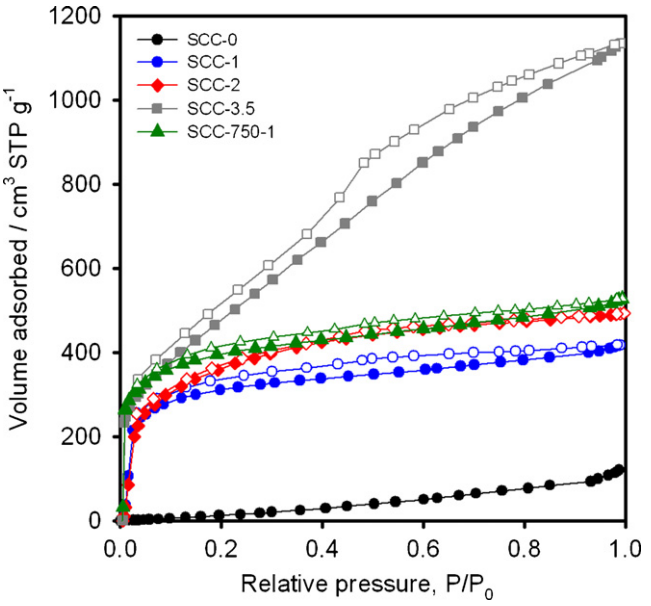

Fig. 2. N_2 adsorption/desorption isotherms (closed/open symbols) at −196 °C for activated carbons obtained from sugar cane bagasse with different $ZnCl_2$ to bagasse impregnation ratios.

prepared at 900 °C without $ZnCl_2$ (SCC-0) presents an adsorption isotherm typical of a non-porous material. By contrast, the four activated carbons prepared using $ZnCl_2$ adsorb much greater volumes of N_2 than SCC-0. Activated carbons SCC-1 and SCC-2 display Type 1 isotherms, which are characteristic of microporous materials, and Type H4 hysteresis loops of slit-shaped pores [22]. Although the isotherms indicate that SCC-1 and SCC-2 are predominantly microporous, the continued slope of the isotherms above a relative pressure of 0.3 suggests the presence of mesopores in these activated carbons. The N_2 sorption data are summarised in Table 2. The total pore volume and specific surface area of the activated carbons increases with the $ZnCl_2$ to bagasse ratio, with SCC-3.5 containing the largest pore volume.

The DFT pore-size distributions in Fig. 3 show that most of the additional pore volume developed in the activated carbons at higher $ZnCl_2$ ratios is due to the growth of pores wider than 2 nm. This trend in the $ZnCl_2$ activated bagasse experiments is consistent with the mechanism of pore widening reported in the literature [13,20]. The volume of narrow micropores, less than 1 nm, is not influenced strongly by the $ZnCl_2$ to bagasse ratio (Fig. 3a).

The specific surface area of bagasse carbon activated by $ZnCl_2$ decreases as the activation temperature increases from 750 to 900 °C, as shown in Table 2. This result is consistent with trends found in other studies of the $ZnCl_2$ carbon activation process [13,23]. The reduction in both surface area and pore volume as activation temperature increases to 900 °C results from $ZnCl_2$ volatilization and a pore shrinkage effect [23]. The TGA curve in Fig. 1b shows that the peak weight-loss steps for bagasse + $ZnCl_2$

Table 2
Surface texture properties of activated carbons from sugar cane bagasse.

Sample	Weight ratio of $ZnCl_2$ to bagasse	Carbon yield (wt.%)	S_{BET} ($m^2\ g^{-1}$)	Pore volume ($cm^3\ g^{-1}$)	[a]Micropore volume ($cm^3\ g^{-1}$)	[a]Mesopore volume ($cm^3\ g^{-1}$)	[b]Narrow micropore volume ($cm^3\ g^{-1}$)
SCC-0	0	19.5	<10	0.18	–	–	–
SCC-1	1	24.3	1155	0.64	0.38	0.26	0.28
SCC-2	2	34.8	1373	0.76	0.54	0.23	0.25
SCC-3.5	3.5	34.2	1788	1.74	0.19	1.55	0.19
SCC-750-1	1	24.7	1452	0.81	0.48	0.33	0.27

[a] Micropore and mesopore volumes calculated from *t*-plot method with carbon black reference.
[b] Narrow micropore volume calculated with Dubinin–Radushkevich method from CO_2 adsorption isotherm at 0 °C.

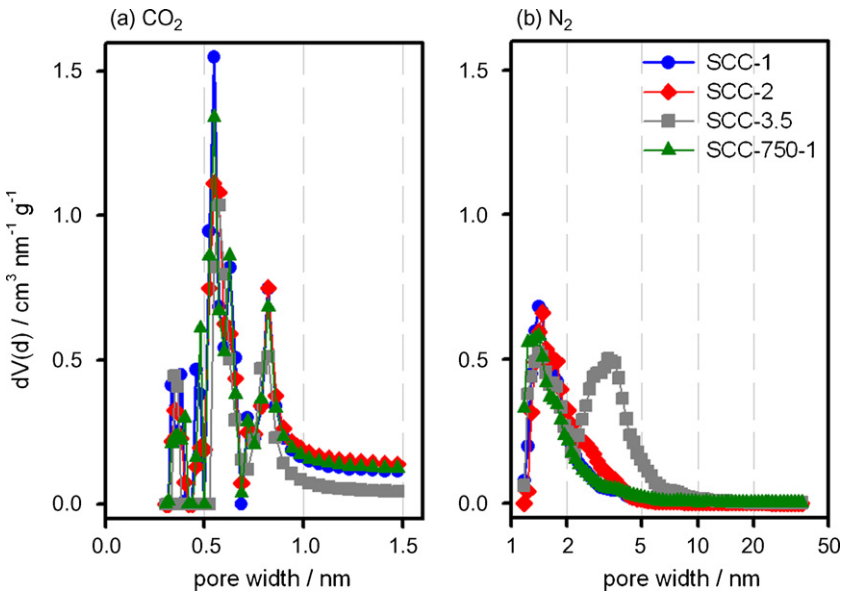

Fig. 3. Pore-size distributions of activated carbons obtained from sugar cane bagasse. Pore-size distribution calculated using density functional theory methods from (a) CO_2 and (b) N_2 sorption analyses.

occur below 620 °C, but temperatures greater than 620 °C continue to produce a slight weight loss. This high temperature weight loss is accompanied by reorganisation of the carbon structure and shrinking of the carbon particles [23]. $ZnCl_2$ has a boiling point of 732 °C [18] so without the $ZnCl_2$ particles to support the carbon pore structure, the carbon structural changes with heat treatment cause shrinkage of the carbon pores. Although $ZnCl_2$ activation at temperatures less than 600 °C may produce maximum surface area [13], the carbon conductivity increases with activation temperatures above 700 °C due to increased orientation of the graphitic carbon structure. The improvement in carbon conductivity with activation temperature can have a positive effect on electrochemical double-layer capacitance [24], despite reductions in surface area.

X-ray photoelectron spectroscopy of activated carbon SCC-1 identified 13 at.% oxygen and 0.2 at.% nitrogen on the carbon surface. The other SCCs feature similar XPS spectra to SCC-1 and thereby suggest that, within the parameters of these experiments, $ZnCl_2$ to bagasse ratio and activation temperature (750–900 °C) do not have a large effect on the oxygen and nitrogen functional groups. The deconvolution of the O1s spectra for SCC-1 is presented in Table 3. Most of the oxygen is distributed in phenol or ether groups and as chemisorbed O_2/H_2O [25]; only a relatively small amount is observed as the electrochemical active quinone form [26]. The distribution of oxygen functional groups is similar for the other SCCs.

Activated carbon SCC-1 was examined using TGA in an air atmosphere up to 750 °C. The carbon weight loss from SCC-1 in air is 96 wt.%. Sugar cane bagasse has an ash content of several percent weight (2.8 wt.% reported by Castro et al. [27]), with a high proportion of silica in the ash [28]. The grey material (4 wt.% of carbon sample) that remains from SCC-1 after TGA in air is a residue of the silica and other mineral ashes present in the raw bagasse. The presence of silica and alumina is confirmed by two low binding-energy peaks (at 155.6 and 106.4 eV) in the wide survey XPS spectrum, in addition to peaks for C1s, O1s and N1s. The low binding-energy peaks can be attributed to Si and Al impurities. These results suggest that the bagasse demineralisation (in water at 100 °C) and carbon rinsing (in 0.2 M HCl at room temperature) procedures do not completely remove silica or alumina from the bagasse and SCC.

3.3. Electrochemical measurements

The activated carbon prepared without $ZnCl_2$ (SCC-0) presents a narrow CV profile, as shown in Fig. 4a. The poor electrochemical performance of SCC-0 results from the low surface area and low pore volume of this carbon. By contrast, the activated carbons prepared with $ZnCl_2$ have well-developed pore structures and exhibit much higher current responses than SCC-0 at a scan rate of 5 mV s^{-1} (Fig. 4a). The rectangular shape of the CV profiles for SCC-1 and SCC-3.5 is characteristic of ideal electrochemical double-layer capacitance. The CV profiles of SCC-2 and SCC-1-750 are not shown in Fig. 4a as the CV responses of these carbons are almost identical to that of SCC-3.5 at 5 mV s^{-1}. At a scan rate of 100 mV s^{-1} the CV curves in Fig. 4b of the four $ZnCl_2$ activated bagasse samples are distinguishable from each other, with SCC-3.5 retaining the most rectangular CV profile. In order of decreasing rectangular shape, the CV profiles are SCC-3.5 > SCC-2.0 > SCC-1-750 > SCC-1.

The three-electrode CV profile of SCC-1 shown in Fig. 5 contains only very small current peaks at around 0.3–0.4 V, which is consistent with the two-electrode CV profiles. The three-electrode CV profile confirms that the concentration of electrochemically active surface functional groups observed by XPS analysis (Table 3) is too low to have a significant impact on the capacitance of SCC-1.

Typical GC profiles of SCC prepared with $ZnCl_2$ activation are presented in Fig. 6. The charge–discharge profiles are symmet-

Table 3
Relative concentrations of oxygen functionalities of SCC-1 obtained by deconvolution analyses of high-resolution X-ray photoelectron spectra.

Sample	O1s		
	Carbonyl-quinone	Phenol–ether	Chemisorbed O_2/H_2O
Binding energy (eV)	531	533	535
at.%	8.7	78.9	12.3

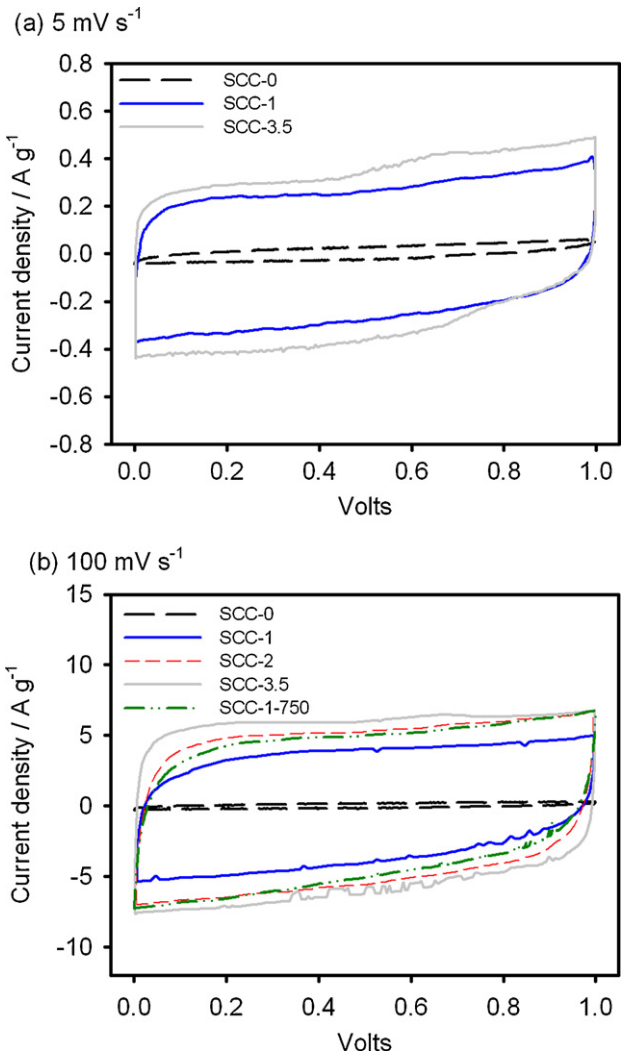

Fig. 4. Cyclic voltammetry of activated carbons from sugar cane bagasse measured in two-electrode cells at (a) 5 mV s^{-1} and (b) 100 mV s^{-1}.

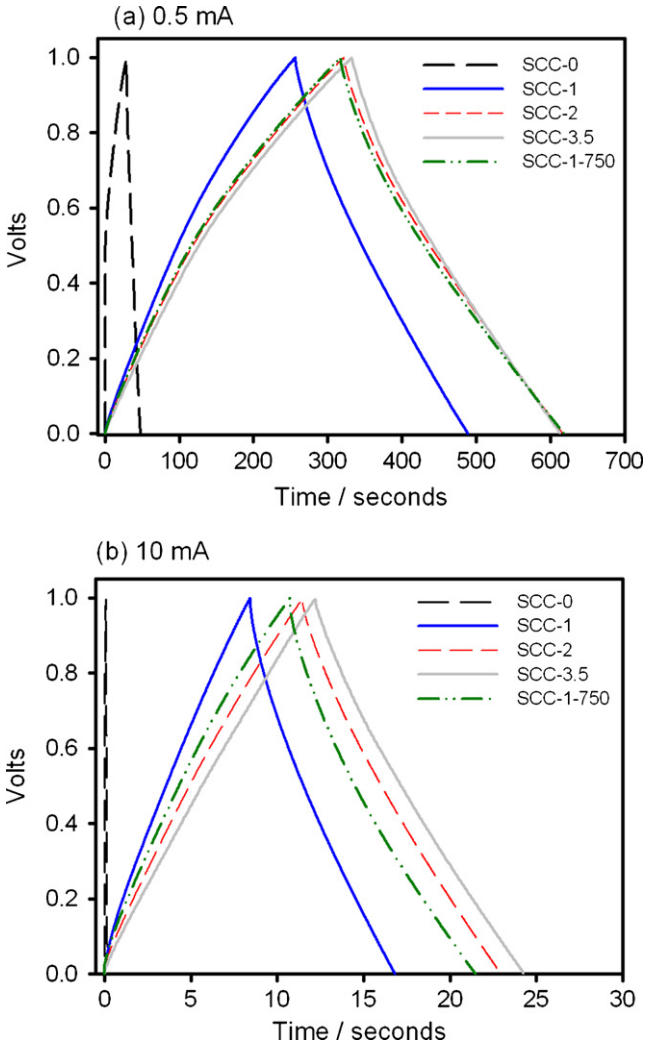

Fig. 6. Typical charge–discharge at (a) 0.5 mA and (b) 10 mA of activated carbons from sugar cane bagasse.

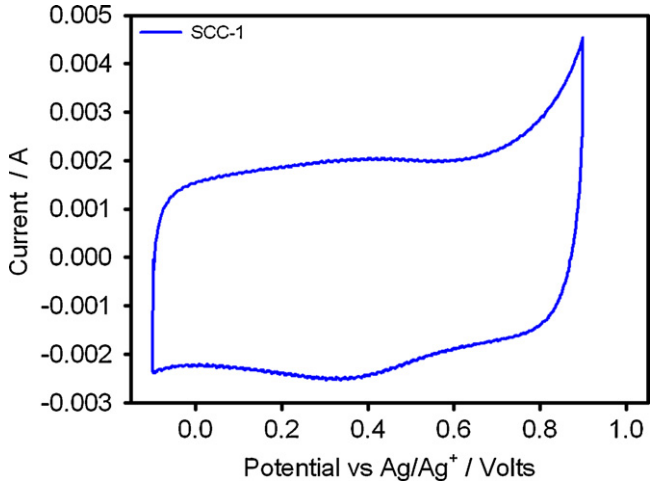

Fig. 5. Cyclic voltammetry for SCC-1 in a three-electrode cell with Ag^+/AgCl reference electrode.

rical, with low *iR* voltage drops and are therefore characteristic of an electrochemical double-layer capacitor. The GC profile for SCC-0 exhibits a large *iR* drop at only 0.5 mA and poor capacitance behaviour at faster current loads. The specific capacitance of the carbon electrodes was calculated from the discharge side of the GC profiles and the values at increasing current loads are shown in Fig. 7a. At low current loads, SCC-1-750 gives the highest specific capacitance (more than 300 F g^{-1}), which is excellent for an activated carbon [1,29]. SCC-2 and SCC-3.5 both have specific capacitances close to 300 F g^{-1} at current loads up to 0.25 A g^{-1}. SCC-1 has a specific capacitance of about 230 F g^{-1}, i.e., a lower value consistent with the lower specific surface area of this activated carbon compared with SCCs prepared with higher $ZnCl_2$ ratios.

Although $ZnCl_2$ activation produces carbons with much lower BET surface areas than the NaOH activated carbons (S_{BET} = 2871 m^2 g^{-1}) investigated by Konno et al. [9], the $ZnCl_2$ activated SCCs in the present study show significantly higher specific capacitances than the NaOH activated carbons derived from sugar cane (70–109 F g^{-1} at 100 mA g^{-1}). Further evidence that $ZnCl_2$ activation produces carbons with superior double-layer capacitance to alkali metal activated carbons is provided by the electrochemical performance of $ZnCl_2$ activated carbons from banana fibres listed in Table 1 [8].

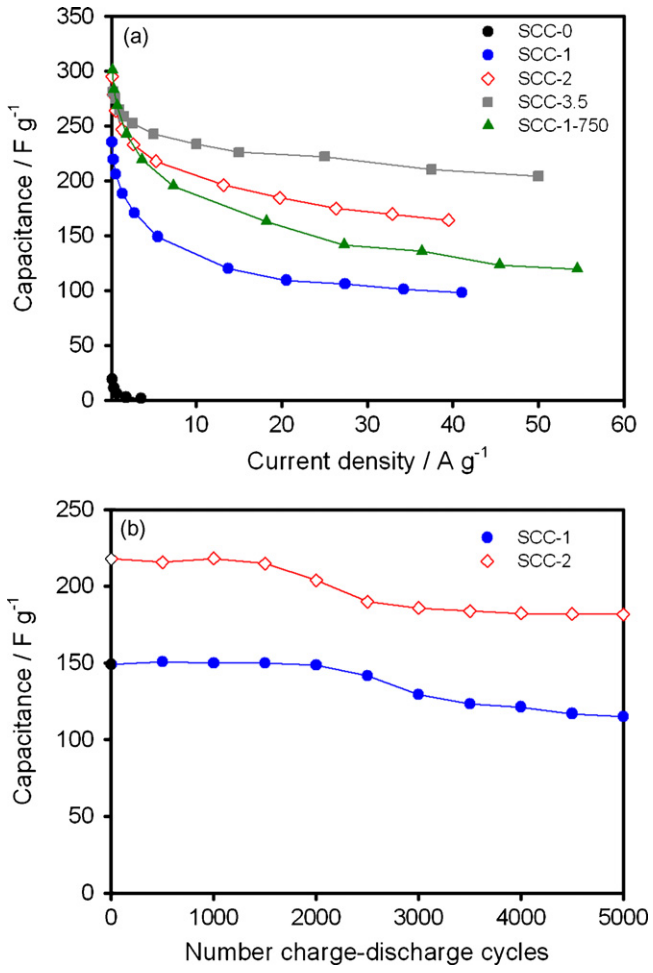

Fig. 7. (a) Influence of current density on specific capacitance of activated carbons obtained from sugar cane bagasse. (b) Charge–discharge cycling stability of SCC-1 and SCC-2 at a current load of 20 mA. Specific capacitance calculated from discharge profiles of galvanostatic cycling curves measured in two-electrode cells.

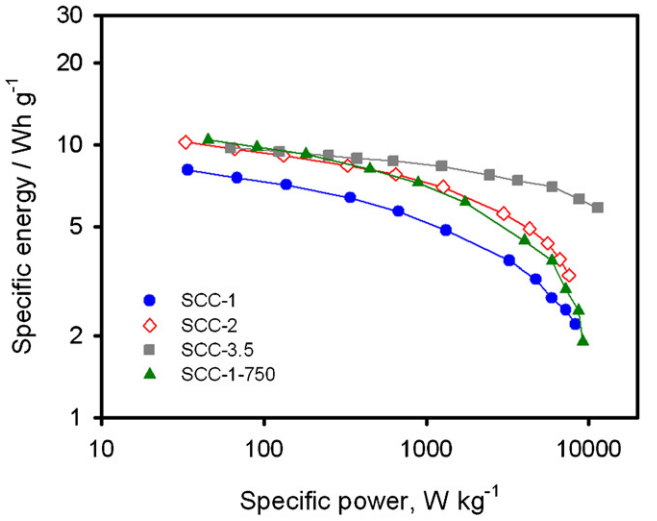

Fig. 8. Ragone plots for activated carbons obtained from sugar cane bagasse. Specific energy and specific power are based on the mass of active electrode material, and exclude the mass of the electrolyte, current collectors and cell packaging.

The enhanced supercapacitor performance obtained with the wider pores developed using $ZnCl_2$, compared with the narrow micropores generally developed using alkali metals, is highlighted by the stable behaviour of the SCCs at fast charge–discharge rates. The specific capacitance at increasing current loads is presented in Fig. 7a. SCC-0 has a value of less than 20 F g^{-1} at the lowest current density measured. At high current loads SCC-3.5 shows the best retention of capacitance. For carbons prepared at 900 °C, the trend in capacitance retention above current loads of 2 A g^{-1} is: SCC-3.5 > SCC-2 > SCC-1. SCC-3.5 has the greatest mesopore volume and gives the most stable double-layer capacitance at increasing current density. Mesopores are reported to act as reservoirs for electrolyte ions and facilitate ion transport through the carbon pore network at fast charge–discharge rates [30].

Although the capacitance of SCC-1-750 is greater than that of SCC-1 at low current loads (which can be explained by the greater specific surface area of SCC-1-750), the deterioration of specific capacitance for the carbons prepared at 750 and 900 °C is similar. Thus the development of mesopore volume with increasing $ZnCl_2$ ratio has a larger effect on the specific capacitance of SCC than activation temperature in the range of 750–900 °C. This observation suggests that an activation temperature of 750 °C is sufficient, when $ZnCl_2$ is used as a porogen, to achieve adequate carbon electrical conductivity for a supercapacitor electrode prepared from bagasse.

The stability of SCC-1 and SCC-2 during charge–discharge cycling at current densities of approximately 5 A g^{-1}, which represents a current density for a high power application, is presented in Fig. 7b. For SCC-1, the capacitance drops after 5000 cycles to 77% of the first cycle, but after 10 000 cycles the capacitance falls by only another 5% of the capacitance in the first cycle. SCC-2 shows better stability with 83% of the capacitance retained after 5000 cycles. The cycling performance of both SCC-1 and SCC-2 is comparable with other biomass-derived activated carbon electrodes reported in the literature [8], but in the present study cycling performance is measured at a much higher current load.

The suitability of carbons derived from sugar cane bagasse for supercapacitor applications is evaluated in the Ragone plots of Fig. 8. Specific energies of up to 10 Wh kg^{-1} (based on the active carbon mass) are achieved by the SCC supercapacitor cells at low current loads. The highest value is obtained with SCC-1-750, i.e., the carbon with the highest specific capacitance. With increasing specific power, the benefit of mesopores in the carbon electrodes are clearly demonstrated by the stable performance of SCC-3.5, which retains 5.9 Wh kg^{-1} at 10 000 W kg^{-1}.

4. Conclusions

The electrochemical performance of activated carbon electrodes prepared by $ZnCl_2$ activation of sugar cane bagasse has been evaluated. Activated carbons with surface areas of more than 1000 m^2 g^{-1} have been produced and the surface area is found to increase with the $ZnCl_2$ to bagasse weight ratio. The volume of mesopores is also found to increase with the $ZnCl_2$ to bagasse weight ratio. Thermal pyrolysis of sugar cane bagasse without $ZnCl_2$ does not produce a carbon with a well-developed pore structure. The $ZnCl_2$ activated carbons display excellent electrochemical properties, with specific capacitances as high as 300 F g^{-1} observed in supercapacitor cells containing 1 M H_2SO_4 electrolyte. The carbon prepared at 750 °C with a $ZnCl_2$ to bagasse ratio of 1 (SCC-1-750) delivers the highest specific capacitance at low current loads. At current densities greater than 1 A g^{-1}, however, the most stable electrochemical performance and the highest specific capacitance is observed for the carbon prepared with the largest $ZnCl_2$ ratio, SCC-3.5. These electrochemical results demonstrate the benefit of mesopores to double-layer capacitance at fast charge–discharge rates.

Acknowledgements

This work was supported financially by the Australian Research Council Centre of Excellence for Functional Nanomaterials. The assistance of Dr Barry Wood with the XPS analysis is greatly appreciated.

References

[1] E. Frackowiak, F. Béguin, Carbon 39 (2001) 937–950.
[2] A. Burke, Electrochim. Acta 53 (2007) 1083–1091.
[3] E. Raymundo-Piñero, F. Leroux, F. Béguin, Adv. Mater. 18 (2006) 1877–1882.
[4] T.E. Rufford, D. Hulicova-Jurcakova, Z. Zhu, G.Q. Lu, Electrochem. Commun. 10 (2008) 1594–1597.
[5] T.E. Rufford, D. Hulicova-Jurcakova, E. Fiset, Z. Zhu, G.Q. Lu, Electrochem. Commun. 11 (2009) 974–977.
[6] F.-C. Wu, R.-L. Tseng, C.-C. Hu, C.-C. Wang, J. Power Sources 144 (2005) 302–309.
[7] M.S. Balathanigaimani, S. Wag-Guen, M.-J. Lee, C.-H. Kim, J.-W. Lee, H. Moon, Electrochem. Commun. 10 (2008) 868–871.
[8] V. Subramanian, C. Luo, A.M. Stephan, K.S. Nahm, S. Thomas, B. Wei, J. Phys. Chem. C 111 (2007) 7527–7531.
[9] K. Konno, Y. Ohba, K. Onoe, T. Yamaguchi, Tanso 231 (2008) 2–7.
[10] C. Ng, J.N. Losso, W.E. Marshall, R.M. Rao, Bioresour. Technol. 84 (2002) 177–185.
[11] M. Valix, W.H. Cheung, K. Zhang, Adsorption 14 (2008) 711–718.
[12] N. Syna, M. Valix, Miner. Eng. 16 (2003) 511–518.
[13] A. Ahmadpour, D.D. Do, Carbon 35 (1997) 1723–1732.
[14] D. Kalderis, D. Koutoulakis, P. Paraskeva, E. Diamadopoulos, E. Otal, J. Olivares del Valle, C. Fernández-Pereira, Chem. Eng. J. 144 (2008) 42–50.
[15] D. Qu, H. Shi, J. Power Sources 74 (1998) 99–107.
[16] M.M. Nassar, E.A. Ashour, S.S. Wahid, J. Appl. Polym. Sci. 61 (1996) 885–890.
[17] S. Munir, S.S. Daood, W. Nimmo, A.M. Cunliffe, B.M. Gibbs, Bioresour. Technol. 100 (2009) 1413–1418.
[18] W.T. Tsai, C.Y. Chang, S.L. Lee, S.Y. Wang, J. Therm. Anal. 63 (2001) 351–357.
[19] L.C.A. Oliveira, E. Pereira, I.R. Guimaraes, A. Vallone, M. Pereira, J.P. Mesquita, K. Sapag, J. Hazard Mater. 165 (2008) 87–94.
[20] M. Molina-Sabio, F. Rodríguez-Reinoso, Colloids Surf. A. 241 (2004) 15–25.
[21] F. Rodríguez-Reinoso, M. Molina-Sabio, Carbon 30 (1992) 1111–1118.
[22] K.S.W. Sing, D.H. Everett, R.A.W. Haul, L. Moscou, R.A. Pierotti, J. Rouquérol, T. Siemieniewska, Pure Appl. Chem. 57 (1985) 603–619.
[23] F. Caturla, M. Molina-Sabio, F. Rodríguez-Reinoso, Carbon 29 (1991) 999–1007.
[24] J. Zhao, Y. Dai, J. Xu, S. Chen, J. Xie, J. Electrochem. Soc. 155 (2008) A475–A480.
[25] S. Biniak, G. Szymański, J. Siedlewski, A. Światlowski, Carbon 35 (1997) 1799–1810.
[26] H.A. Andreas, B.E. Conway, Electrochim. Acta 51 (2006) 6510–6520.
[27] J.B. Castro, P.R. Bonelli, E.G. Cerrella, A.L. Cukierman, Ind. Eng. Chem. Res. 39 (2000) 4166–4172.
[28] W.T. Tsai, C.Y. Chang, M.C. Lin, S.F. Chien, H.F. Sun, M.F. Hsieh, J. Environ. Sci. Health B B36 (2001) 365–378.
[29] A.G. Pandolfo, A.F. Hollenkamp, J. Power Sources 157 (2006) 11–27.
[30] D.-W. Wang, F. Li, M. Liu, G.Q. Lu, H.-M. Cheng, Angew. Chem. Int. Ed. 47 (2008) 373–376.